

Analysis of Earthquake Recordings Obtained from the Seafloor Earthquake Measurement System (SEMS) Instruments Deployed off the Coast of Southern California

by David M. Boore and Charles E. Smith

Abstract For more than 20 years, a program has been underway to obtain records of earthquake shaking on the seafloor at sites offshore of southern California, near oil platforms. The primary goal of the program is to obtain data that can help determine if ground motions at offshore sites are significantly different than those at onshore sites; if so, caution may be necessary in using onshore motions as the basis for the seismic design of oil platforms. We analyze data from eight earthquakes recorded at six offshore sites; these are the most important data recorded on these stations to date. Seven of the earthquakes were recorded at only one offshore station; the eighth event was recorded at two sites. The earthquakes range in magnitude from 4.7 to 6.1. Because of the scarcity of multiple recordings from any one event, most of the analysis is based on the ratio of spectra from vertical and horizontal components of motion. The results clearly show that the offshore motions have very low vertical motions compared to those from an average onshore site, particularly at short periods. Theoretical calculations find that the water layer has little effect on the horizontal components of motion but that it produces a strong spectral null on the vertical component at the resonant frequency of P waves in the water layer. The vertical-to-horizontal ratios for a few selected onshore sites underlain by relatively low shear-wave velocities are similar to the ratios from offshore sites for frequencies less than about one-half the water layer P -wave resonant frequency, suggesting that the shear-wave velocities beneath a site are more important than the water layer in determining the character of the ground motions at lower frequencies.

Introduction

The data analyzed in this article were obtained from instrumentation installed on the seafloor by the Seafloor Earthquake Measuring System (SEMS) project. The objective of this system is to obtain ground shaking data on the seafloor that can be used to evaluate the design of offshore oil platforms. In particular, a key question is whether the ocean bottom motions are fundamentally different than those at onshore locations. If so, then the more abundant strong-motion onshore data may be inapplicable for the specification of design motions for offshore platforms. This article uses SEMS data obtained through 1997 to answer this question.

The SEMS instrument development, deployment, and data recovery were carried out by Sandia National Laboratory, with funding from the Minerals Management Service. The SEMS was developed in a number of stages, although all stages used digital recording. In this article, we refer to these stages as SEMS1, SEMS2, SEMS3, and SEMS4 (or more briefly, S1, S2, S3, and S4). In all stages, a three-axis ac-

celerometer was embedded several meters below the seafloor, and the output from the accelerometer was fed either to a self-contained instrument package resting on the seafloor (SEMS1, SEMS2, and SEMS3) or via a cable to a datalogger on a nearby oil platform (SEMS3 and SEMS4). The data acquisition units for the first three SEMS stages used 16-bit digitizing at 100 samples per second; the SEMS4 unit used 24-bit digitizing at 20 samples per second. A history of the SEMS is contained in Reece *et al.* (1981), Ryerson (1981), Sleaf and Engi (1987), Sleaf (1990), Smith (1990, 1991, 1994), and Boore (1997).

Because of the lack of onshore data for distances comparable to those from the source to the SEMS sites, the empirical interpretation of the data focused on the ratio of response spectra for the vertical and horizontal components (V/H) as a function of period. Comparisons to the few available ratios and to the ratios derived from regression analysis of strong-motion data clearly shows the offshore ground motions to have anomalously low ratios for short-period

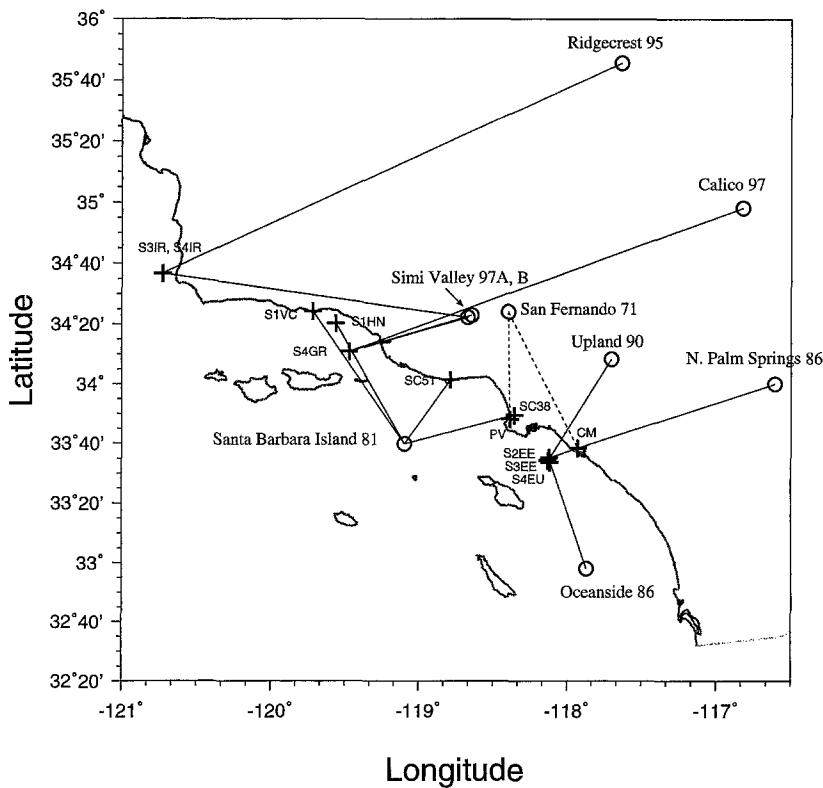


Figure 1. Map of southern California. Lines connect events (open circles) and stations (pluses) providing data for the corresponding event. The dashed lines show paths for two recordings of the 1971 San Fernando earthquake; these paths cross the Los Angeles basin, as does the path from the Upland 1990 earthquake to SEMS site S3EE. Waveforms of these two events are compared in this article. Although providing no data, station S4EU is shown for completeness.

- With one exception, each earthquake was recorded on only one of the offshore SEMS stations. The exception is the first Simi Valley, 1997, aftershock of the 1994 Northridge earthquake. This event was recorded on two SEMS4 stations: S4GR and S4IR. The lack of multiple offshore recordings for a given event limits, to an extent, the interpretation of the data.
- A more important limitation than the lack of multiple offshore recordings is the relative scarcity of onshore data at sites near the offshore sites. (By near, we mean along the same general azimuth from the earthquake to the SEMS site, and at distances as close to the SEMS site as the coastal configuration allows; for the earthquakes listed in Table 3, there are generally numerous recordings of ground motion but at epicentral distances much smaller than the epicentral distances to the SEMS stations.) Most of the SEMS records were obtained from moderate-size earthquakes at distances in excess of 70 km. The standard analog, onshore accelerographs do not have the sensitivity to provide digitizable data at these distances for the earthquakes recorded on the SEMS sites. The only earthquake for which we were able to obtain onshore and offshore data is the Santa Barbara Island, 1981, earthquake, which was recorded on three onshore stations, one of which was a SEMS unit installed onshore, near Vic Trace Reservoir. The other two recordings, SC38 and SC51, were obtained on standard analog accelerometers maintained by the University of Southern California (USC). Only recently have onshore instruments with performance characteristics comparable to those of

the SEMS units been installed in the southern California region.

- Several sites recorded different earthquakes, thus allowing a check on the stability of the ratio of motions on the vertical and horizontal components. These sites include S2EE, with two recordings; S4GR, with three recordings; and S4IR, with two recordings. In addition, sites S2EE and S3EE were close to one another, so if counted as one site, three recordings are available for these sites.

Other earthquakes than those listed in Table 2 have been recorded by the SEMS units. There have been smaller earthquakes than those used in this study (e.g., Reece *et al.*, 1981, discuss data from a magnitude 3.2 earthquake recorded at S1HN and S1VC), but none of these data were available to us. In addition to the SEMS stations, several platforms have been instrumented by the oil company responsible for the platform, and apparently, data from these installations have been obtained. For example, Chen *et al.* (1989) and Mason *et al.* (1989) discuss records on and beneath platform Grace obtained from the 1987 Whittier Narrows earthquake (this event was not recorded on any SEMS stations).

Processing of Accelerograms

The accelerograms required minimal processing. The S2EE recordings were corrected for an inadvertent low-cut filter (3 db down at 1 Hz), and all records were filtered to remove low-frequency noise. The choice of low-cut filters (f_c) was based on examination of whole-record Fourier spec-

tral amplitudes (Fig. 2 shows some sample spectra). Much of the analysis is based on 5%-damped pseudovelocity response spectra (*PSV*) computed from the accelerograms, where $PSV = 2\pi f S_d$, and S_d is the maximum displacement response of a 5%-damped single-degree-of-freedom harmonic oscillator with resonant frequency f driven by the particular accelerogram (see, e.g., Hudson, 1979). Numerical experiments showed that the response spectra computed from the accelerograms are not sensitive to the choice of the cutoff frequencies for oscillator periods less than $0.5/f_c$. We have generally used response spectra for periods less than or equal to 2.0 sec, using the cutoff frequencies given in Table 4.

The Character of the Waveforms

Visually, the accelerograms recorded on the SEMS units look much like those from onshore sites. As an example, Figure 3a shows three components of motion for the 1990 Upland earthquake ($M = 5.6$); because the units have pre-event buffers, the initial *P*-wave motion has been captured (unlike the records from analog accelerographs), and the *P* wave is followed by a clear *S* arrival, which is followed by a slowly decaying coda or tail. The vertical component is small relative to horizontal components, but it is possible to find onshore records with comparable relations between the components.

The acceleration, velocity, and displacement time series for the 1990 Upland SEMS recording are also shown in Figure 3. The acceleration traces are largest near the beginning of the record, and they decay to small motions at the time of arrival of the large-amplitude long-period waves. The outstanding feature of these figures is the late-arriving, long-period (≈ 6 sec) motion on all three components. This motion is not unexpected, for the travel path (Fig. 1) traverses the Los Angeles basin, and the waves resemble the surface waves that have been observed to propagate in the basin. In seismological terms, the peak accelerations are probably carried by body waves, while the long-period arrivals are surface waves.

The ground motions from the SEMS recording of the 1990 Upland earthquake are similar to those from the 1971 San Fernando earthquake ($M = 6.6$) recorded at sites for which the waves have traveled comparable distances through the Los Angeles basin, as shown in Figure 4 (in which we have chosen the horizontal component from each record that best matches the various records). The stations, earthquake location, and paths are shown in Figure 1. The records are in good qualitative agreement: the displacements increase in time, with the largest displacements occurring 45 to 60 sec after the initial *S* arrival. The peak displacements are carried by waves with periods near 5 sec. Exact agreement of the waveforms for the various recordings is not expected; the earthquakes were different in magnitude and in travel path. The source duration for the Upland earthquake was probably shorter than the period of dominant displacement motion,

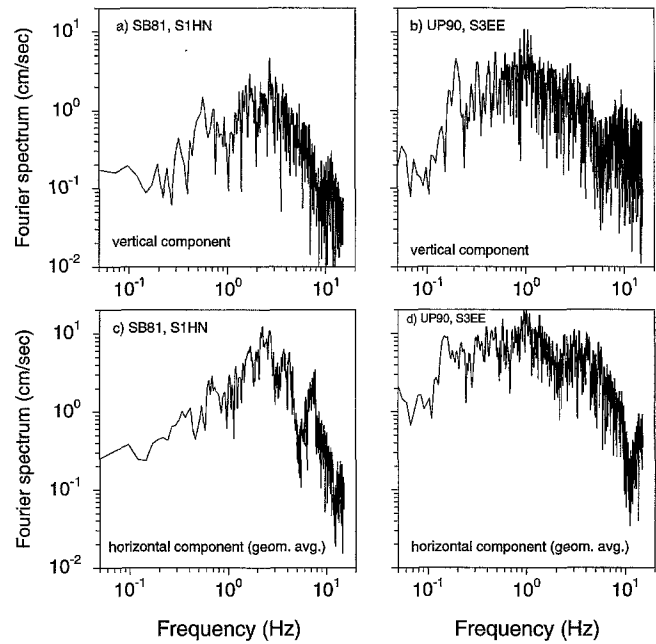


Figure 2. Uncorrected, unsmoothed whole-record Fourier amplitude spectra for SEMS recordings of the two earthquakes recorded at SEMS offshore sites S1HN and S3EE. For clarity, the spectra for the two horizontal components have been replaced by the geometric average of the individual spectra.

Table 4
Low-Cut Filter Frequencies Used in Making the Plots of
Velocity and Displacement Time Series

EqCode	StaCode	LC freq
SB81	S1HN	0.2
SB81	S1VC	0.2
SB81	SC38	0.2
SB81	SC51	0.2
NP86	S2EE	0.5
OS86	S2EE	0.5
UP90	S3EE	0.1
RC95	S4IR	0.2
CL97	S4GR	0.1
S97A	S4GR	0.1
S97A	S4IR	0.1
S97B	S4GR	0.1

but this is not the case for the San Fernando recordings, for which the source duration and the period of dominant displacements are comparable.

As an aside, we note that recorded durations from instruments triggered on acceleration levels (such as the ubiquitous analog strong-motion accelerographs) might be too short to capture the peak displacements. If the duration of recording following the initial trigger is set to less than about 60 sec, then it is possible that the largest displacements will not be recorded.

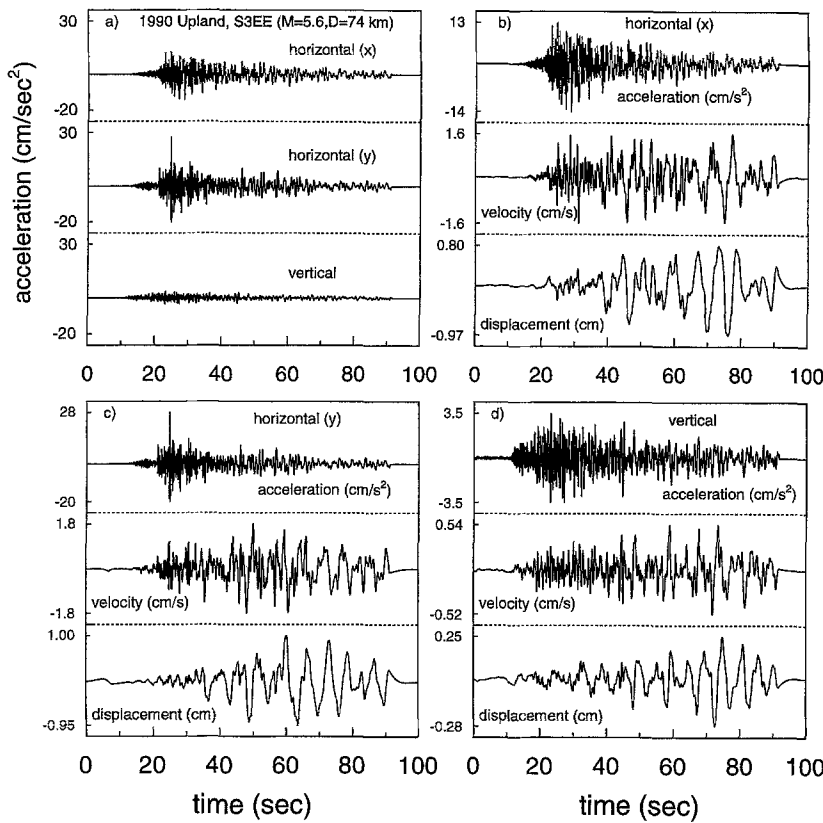


Figure 3. (a) Three-component-accelerograms (in cm/sec^2) of the Upland 1990 earthquake recorded at SEMS station S3EE, plotted using the same vertical scale to emphasize the relative amplitude of the components. (b), (c), and (d) Acceleration (cm/sec^2), velocity (cm/sec), and displacement (cm) time series for the three components of the S3EE recording of the 1990 Upland earthquake, plotted using different vertical scales, to emphasize the appearance of the waveforms. Note the dominance of late-arriving 5 to 6 sec waves on the displacement trace, something not readily seen in the accelerogram.

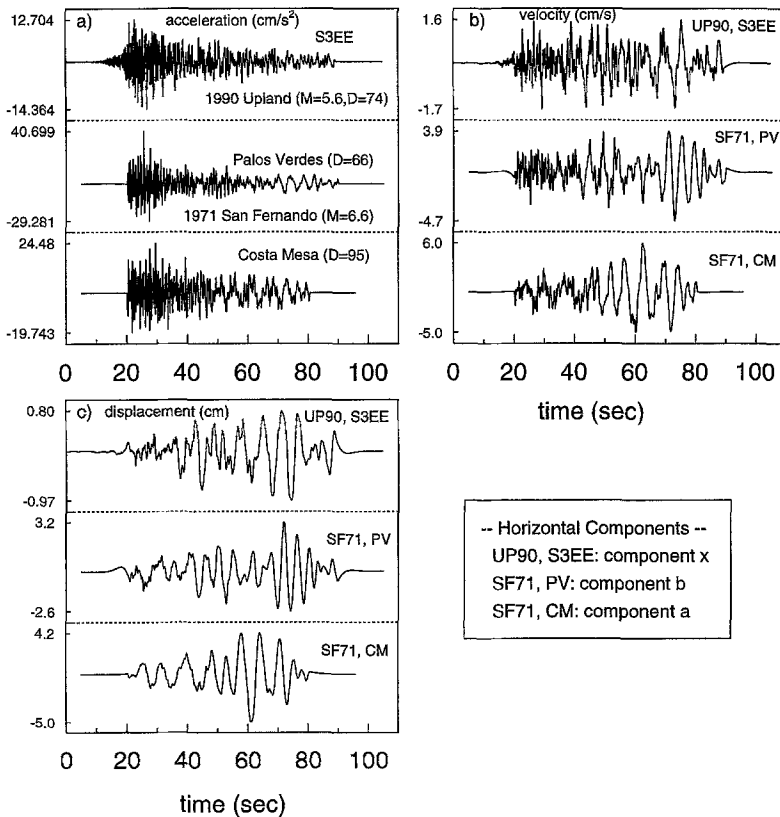


Figure 4. Horizontal-component accelerations (cm/sec^2), velocities (cm/sec), and displacements (cm) from the 1990 Upland earthquake recorded offshore at S3EE (*top trace*) and from the larger 1971 San Fernando earthquake recorded at Palos Verdes and Costa Mesa (*middle and bottom traces*, respectively), aligned on the *S* arrival. The accelerograms were low-cut filtered at 0.1 Hz before integration to velocity and displacement. The two 1971 recordings apparently triggered on the *S* wave, but it is unlikely that the response spectra at the longer periods will be affected by the short duration of missing *S* energy. The durations of the accelerograms represent the complete recording, after which the triggered instruments turned off. The long-period energy probably continued for a longer duration.

V/H —Observations

The main goal of the SEMS program is to study the similarities and differences between seafloor and onshore ground motions. Because the earthquakes recorded at the SEMS sites were generally not recorded at nearby onshore sites, it is difficult to make a direct assessment of the agreement between onshore and offshore motions; ground motions depend on many variables, such as earthquake size and type of faulting, distance from the source, propagation path, and local site geology, and a comparison of only a few recordings is worthless unless adequate corrections can be made to remove these influences on the amplitudes of the motions. The ratio of vertical to horizontal motions (V/H), however, might be expected to remove all but the effect of local geology, at least to first order (Atakan and Havskov, 1996, have used this method to determine site response on the ocean floor under the North Sea). By using ratios, it is possible to compare a few onshore and offshore recordings to see if they were comparable. We also compare the ratios from offshore recordings with those predicted from regression analyses based on hundreds of onshore recordings from many earthquakes; this provides a measure of comparison that represents the average ratio for a typical site and earthquake of a specified magnitude and distance. In addition, we compare the average V/H for offshore SEMS sites to V/H from a few onshore recordings for which the shear-wave velocities beneath the recording sites are similar to the velocities we estimate to exist beneath the SEMS offshore sites.

We studied both ratios of Fourier spectra and ratios of response spectra. The Fourier spectra are more directly related to site transfer functions, but the response spectra have the advantage of having relations available from the analysis of numerous onshore recordings, which provide a well-founded mean expectation for onshore recordings.

Effect of Record Duration on V/H . As mentioned earlier, it is not clear that the recorded motions have captured all of the long-period motion. Based on computations of the V/H ratios for various record durations of the longest record available to us, we conclude that response spectral ratios for periods less than about 2.0 sec should be relatively unaffected by late-arriving waves. This cutoff means that long-period basin waves, such as those in the SEMS recording of the 1990 Upland earthquake, will not be included in the analysis.

V/H from Recorded Ground Motions. Because the orientations of the horizontal components were often unknown, we made no attempt to rotate the motions into radial and transverse directions. Instead, we computed V/H ratios for each horizontal component separately. The ratios for each component are similar, and for convenience in presentation, the plots show the geometric mean of the two ratios computed for each horizontal component. Figures 5 and 6 display V/H for sites with recordings of more than one earthquake, where

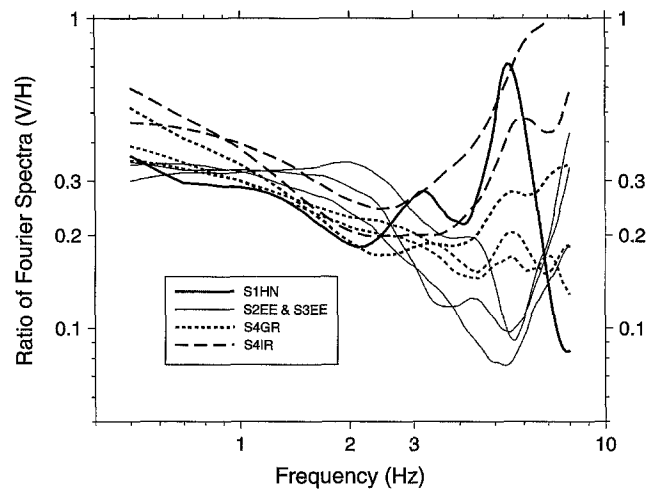


Figure 5. Comparison of V/H ratios of Fourier amplitude spectra for the S -wave portion of the offshore SEMS recordings through 1990. For clarity, the same line type was used for all recordings at a given site, to emphasize the site-to-site variation of the ratios. Spectral ratios were computed after smoothing each component with a triangular operator spanning 2 Hz.

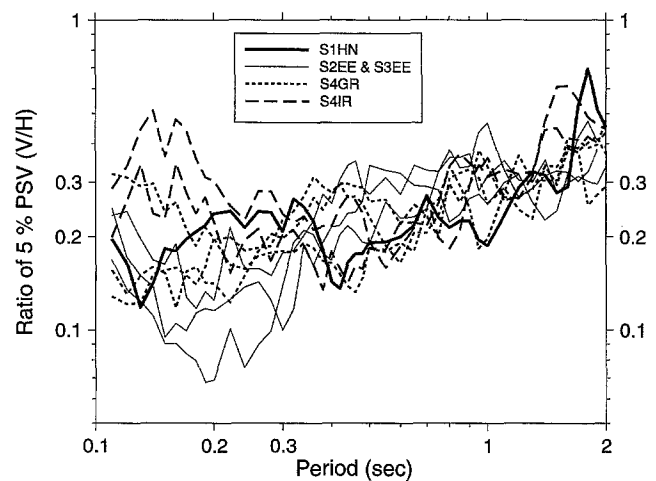


Figure 6. Comparison of V/H ratios of 5%-damped response spectra (PSV) for recordings at all of the offshore SEMS sites considered in this article. The PSV were computed using the complete time series for each recording, but the same values would have been obtained if only the S -wave portion of the time series had been used.

we have treated S2EE and S3EE as one site. There is a general trend for the ratios to increase with period, and there is more scatter at short periods than at long periods. The large scatter at short periods is primarily due to site-to-site variations in the ratio (in particular, compare the S2EE and S3EE to S4IR). The larger differences at short period than at long period are what we expect in view of possible lateral variations in shear-wave velocity and water depth (which we

will show to have a pronounced effect on the spectral ratios at high frequencies), and the similarity of the ratios for different events suggests that the ratios are strongly controlled by local site conditions.

Comparison of V/H from Offshore SEMS and from Onshore Regression Analyses. The average offshore response spectral ratios are compared to regression-based average onshore spectra in this section; ratios of Fourier amplitude spectra are compared to theoretical predictions later in the article. Two recent sets of regression analyses were used to provide onshore ratios of vertical and horizontal components. These are Abrahamson and Silva (1997) and Campbell (1997). The Abrahamson and Silva relations, hereafter referred to as AS97, were derived from data recorded at distances as large as 200 km; in contrast, the Campbell relations (C97) only used data for distances less than or equal to 60 km. Both AS97 and C97 give equations for the vertical and horizontal components separately; we formed V/H from the individual components predictions. In all cases, we show results for soil sites, that is, the average soil site represented by the collection of strong-motion stations. Many of these stations are on stiff soil; the average shear-wave velocity in the upper 30 m (V_{30}) for a typical soil site is 310 m/sec (Boore and Joyner, 1997), based on the analysis of velocities from boreholes, many of which are collocated with strong-motion stations. The shear-wave velocities beneath the SEMS offshore sites are probably lower than at a typical onshore soil site, with $V_{30} \approx 220$ m/sec (as shown later).

The V/H ratios of PSV from recordings of the 1981 Santa Barbara Island earthquake, which was recorded on an offshore station and several onshore stations (Fig. 1), are shown in Figure 7, in which it is clear that the offshore recording (S1HN) has a much different V/H than for the onshore recordings. The difference is largest at short periods and tends to decrease at long periods. The regression-based ratios are in much better agreement with the onshore ratios than with the offshore ratio. The onshore sites are probably underlain by materials with higher shear-wave velocities than is the offshore site (with the exception of SC38, which is described to be on dune sand in Anderson *et al.*, 1981, whereas S1VC and SC51 are on marine terrace deposits), and therefore, we expect the spectral ratios for the onshore sites to be more similar to the ratios from regression-based results than for the offshore site.

A comparison between the regression-based onshore results and the average of the SEMS offshore results is shown in Figure 8. The distance at which the AS97 relations were evaluated was 120 km, which is close to the geometric mean distance of 113 km for the events used in forming the ratio. The regression-based results for C97 were evaluated at the greatest distance—60 km—for which his equations are valid. Also included in the comparison in Figure 8 are results from analyses of specific earthquakes (Loma Prieta 1989 and Northridge 1994), as well as results from the SMART1 array in Taiwan. In general, the onshore results are above the

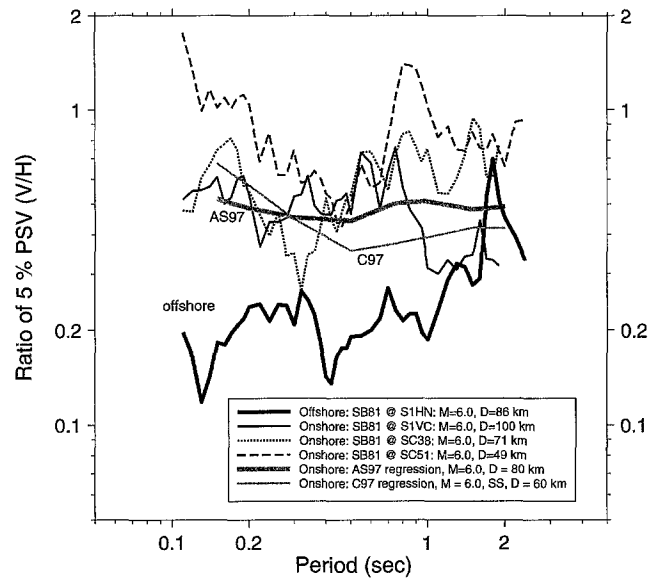


Figure 7. V/H ratios of 5%-damped response spectra for offshore and onshore recordings of the 1981 Santa Barbara Island earthquake, compared with the regression results of Abrahamson and Silva (1997) (AS97) and Campbell (1997) (C97).

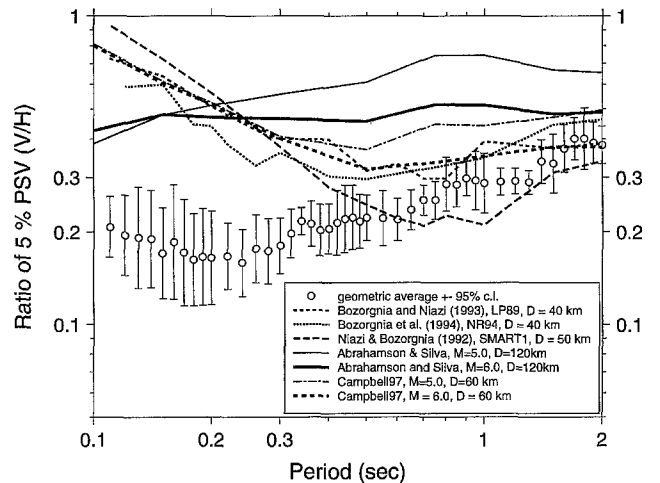


Figure 8. Observed offshore V/H ratios of 5%-damped response spectra (open circles) compared with onshore ratios from regression analyses. The results for the Loma Prieta and Northridge earthquakes are indicated in the legend by “LP89” and “NR94”, respectively. The Bozorgnia *et al.* (1994) results for the Northridge earthquake differ slightly from those in the final published study (Bozorgnia *et al.*, 1995).

SEMS offshore results, and the difference is largest at short periods.

The large difference between average onshore sites and the SEMS offshore recordings at short periods is consistent with the findings of Snee (1990), who made scatter plots of peak accelerations, with horizontal components on one

axis and vertical components on the other. Using different symbols for offshore and onshore recordings, he found two populations separated in the same sense as we found for response spectra. In addition, Smith (1990) found that V/H for peak acceleration and peak velocity from offshore sites was smaller than for onshore sites, again in qualitative agreement with the findings from the spectral ratios.

At longer periods, a difference between AS97 and C97 and the SEMS results still persists, but the difference is much smaller than at short periods. The C97 results are closer to the SEMS results than are the AS97 predictions, but recall that the C97 results are for $D = 60$. The AS97 relations have a distance dependence that produces an increase of V/H with distance for periods greater than about 0.3 sec (see Fig. 23 and 24 in Boore, 1997), which if true for C97 would lead to larger values for $D > 60$ km, and therefore, the C97 ratios would be more discordant with SEMS ratios than shown in the figure. Although the AS97 and C97 ratios are higher than the SEMS ratios at all periods, it may be significant that the SMART1 results produce somewhat lower values of V/H than the SEMS values for periods in excess of about 0.6 sec (and if the distance dependence in the AS97 relations holds for the SMART1 data, then applying a distance correction to go from the ratios at 50 km to the average earthquakes-to-SEMS distance would likely result in the SMART1 ratios being in good agreement with the SEMS ratios). As shown later, the SMART1 site is underlain by low-velocity materials that may be close to those under an average SEMS site, and therefore the SMART1 site may be a closer analog to the average SEMS offshore site than the average soil class represented by the other regression results.

Comparison of V/H from Offshore SEMS and from Selected Onshore Recordings. The relatively good agreement at longer periods between the spectral ratios from the offshore SEMS recordings and the recordings on the SMART1 array suggests that at longer periods the comparison between offshore and onshore ground motions is more a function of the sediments underlying the sites than it is on the presence or absence of a layer of water above a site. We have made a limited test of this suggestion by comparing V/H of offshore and onshore sites underlain with similar velocities. Figure 9 shows velocities estimated at offshore SEMS sites and velocities from several onshore sites: the LSST site within the SMART1 array in Taiwan and three sites in California—two sites near the edge of San Francisco Bay and a site in the Imperial Valley. Between about 10 and 100 m, the estimated SEMS velocity is similar to these onshore sites; three of the onshore sites have lower velocities in the upper 10 m or so (the material in the upper 10 m at these sites is clay, unlike the Imperial Valley site). Three-component acceleration time series for recordings at the California sites are given in Figure 10, along with the offshore recordings of the 1990 Upland earthquake at S3EE. The general character of the time series is similar, but the S3EE recordings have smaller vertical accelerations relative to the horizontal ac-

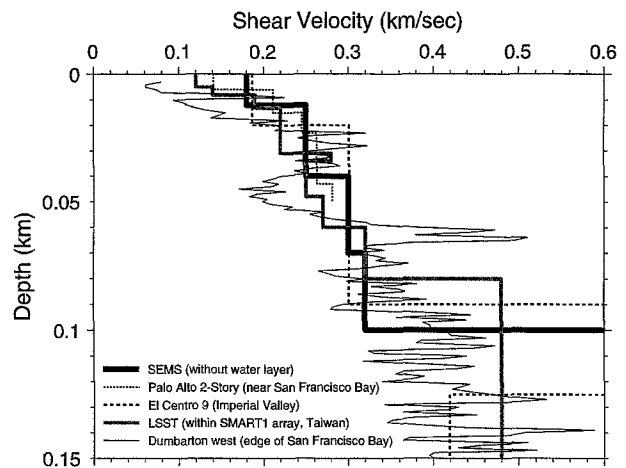


Figure 9. Shear-wave velocity estimated for an average offshore SEMS site and measured at several onshore sites for which the velocities are comparable to the estimated SEMS velocity.

celerations. The ratios of response spectra (Fig. 11) again emphasize the dramatic difference between offshore and onshore ground motions at short periods shown earlier in Figure 8. In contrast to Figure 8, however, the ratios at long periods are generally smaller than those from offshore sites. The difference in long-period ratios in Figures 8 and 11 at onshore sites may be due to the variations in shear-wave velocities beneath the sites—the velocities below the sites used in Figure 11 are much lower than at an average soil site—and gives some support to the idea that V/H at longer periods is strongly controlled by the underlying shear-wave velocities.

Peak Motions as a Function of Distance

The previous figures show a clear difference in V/H at short periods between the offshore and onshore recordings. Is this due to onshore vs. offshore differences in the vertical components, in the horizontal components, or in both? To answer this question, we plot in Figure 12 response spectral amplitudes for a few selected periods as a function of distance from the earthquake, using 1981 Santa Barbara Island data (for which both onshore and offshore data are available). For comparison, the figure includes the regression-based results of AS97 and C97. From these plots, it is clear that the offshore vertical component is always smaller than the onshore vertical components (after accounting for the attenuation with distance); the difference is greatest at short periods. The same is not always true for the horizontal components. This comparison is strong evidence that the very low values of V/H at short periods are due to small values of V , rather than large values of H . A similar conclusion was drawn by Smith (1994), who plotted peak accelerations against distance for vertical and horizontal components.

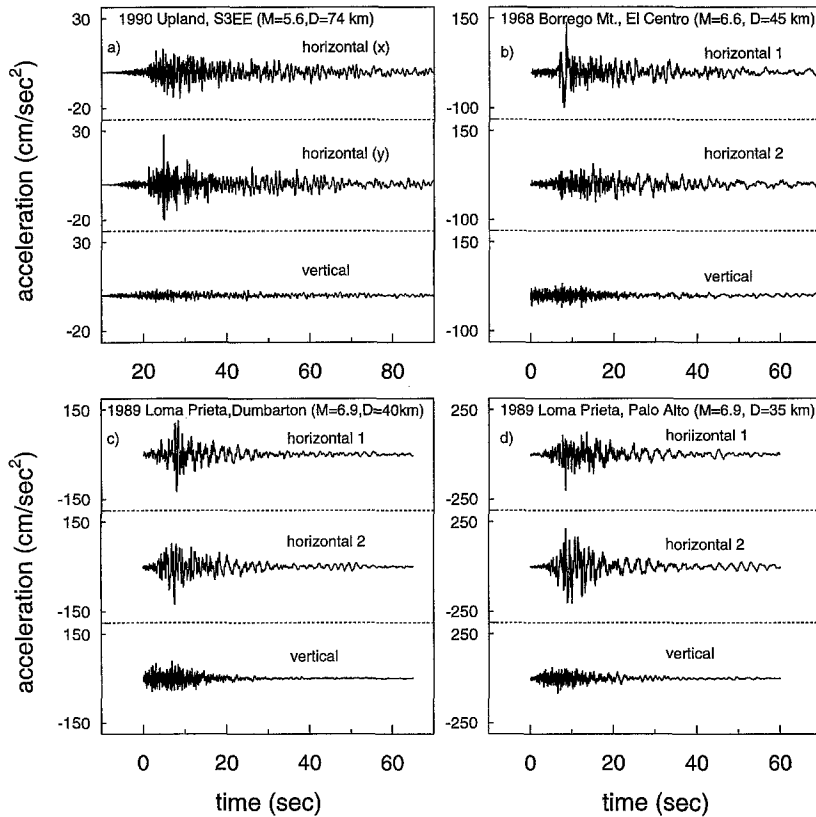


Figure 10. Three-component accelerograms for a SEMS recording (1990 Upland earthquake at S3EE) and three recordings made at onshore sites underlain by shear-wave velocities similar to those estimated to be beneath the SEMS sites.

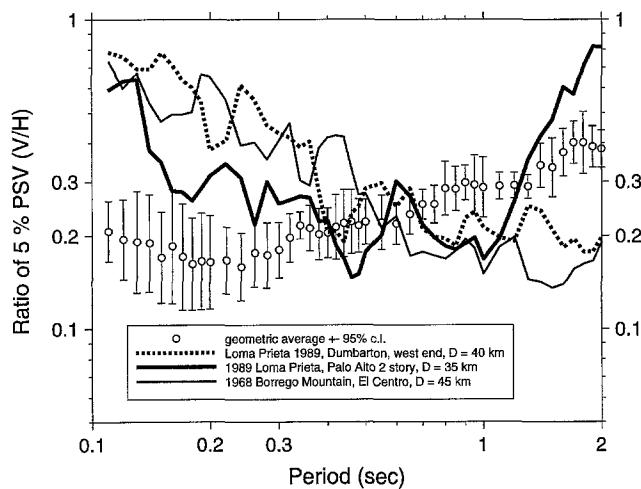


Figure 11. V/H ratios for offshore SEMS sites (open circles) and from three onshore sites underlain by velocities similar to those estimated to lie beneath the SEMS sites.

V/H —Theory

This section presents a comparison of the observed ratios of vertical and horizontal motions with theoretical computations. Such a comparison helps in understanding the physical mechanism leading to the particular observed ratios

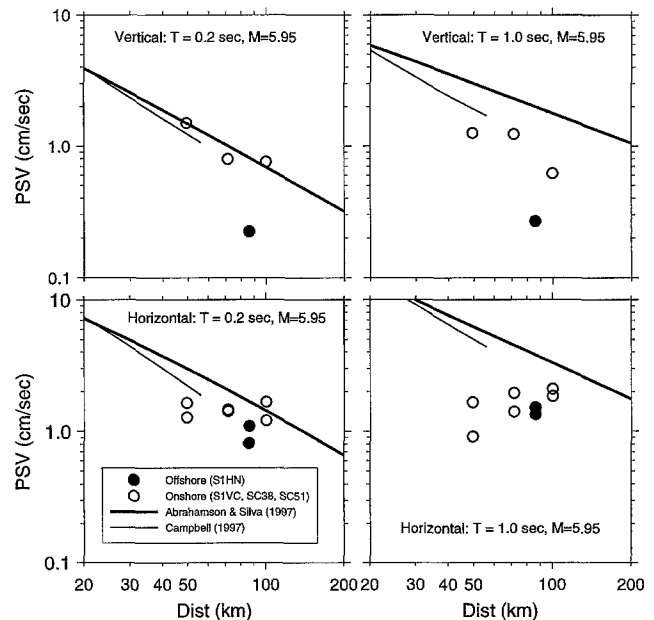


Figure 12. 5%-damped pseudo-velocity response spectra for 0.2- and 1.0-sec oscillator periods as a function of epicentral distance for the 1981 Santa Barbara Island earthquake, compared with predictions from regression analyses, for vertical components (top two panels) and horizontal components (bottom two panels). The symbols differentiate between the offshore and onshore recordings of the earthquake.

and can be used to assess the motions expected in cases for which data are not available.

Velocity Model

The first step in the procedure is to derive velocities as a function of depth below a typical site. Sufficient information was not available to do a site-by-site evaluation, but this should not be an important limitation in view of the overall agreement in the spectral ratios for the SEMS sites. Site-specific velocity structures, however, undoubtedly explain some of the site-to-site variations.

Finding no direct measurements of the velocity, we estimated the velocity from available information and from analogs to other onshore sites for which velocity information is available. The model was divided into three layers: water, 0.1 km of soft sediments, and underlying crust. We did the calculations using various combinations of these three components to understand the influence of each.

Water Layer. The depth of the water in the model is 60 m, which is appropriate for a number of the SEMS sites that we studied (see Table 1).

Shallow Sediments. We obtained lithologic data and standard penetration data for three borings near SEMS station S3EE from reports submitted to the MMS. The logs indicate that most of the sites are underlain by sands and silts, with some clay present (the deeper sites may be subject to less current scouring and may be underlain by more clay—logs near platform Eureka near S4EU support this conjecture). T. Fumal of the USGS estimated shear-wave velocity from this information, based on his experience with correlations between SPT and shear-wave velocities (e.g., Fumal, 1978). His estimates are labeled “hole 261-1,” “hole 216-3,” and “hole 262-1” in Figure 13. Also included on this plot are shear-wave velocities from Hamilton (1976a) for ocean-bottom sediments, velocities determined by L. Dorman (written comm., 1997) for a site offshore of southern California, near Camp Pendleton, and velocities for several sites off the coast of Norway for which the water depths are comparable to those for the SEMS stations (Rognlien, 1987). Based on these velocities for ocean-bottom sites on continental shelves, we derived a model of velocities in the upper 100 m; these velocities are shown in the figure.

The adopted SEMS model is in good agreement with those from onshore boreholes close to Long Beach. Figure 14 shows a map of USGS boreholes in the vicinity, and Figure 15 shows the velocities, along with the SEMS model. The velocities separate into two groups, which the map indicates are well correlated with the age of the near-surface sediments: with one exception (BH16), the lower velocities correspond to Holocene sediments, while the higher velocities correspond to the older Pleistocene sediments (for those sites with Holocene sediments at the surface, BH44 is unusual in that the low-velocity Holocene sediments are underlain by much higher velocity shales).

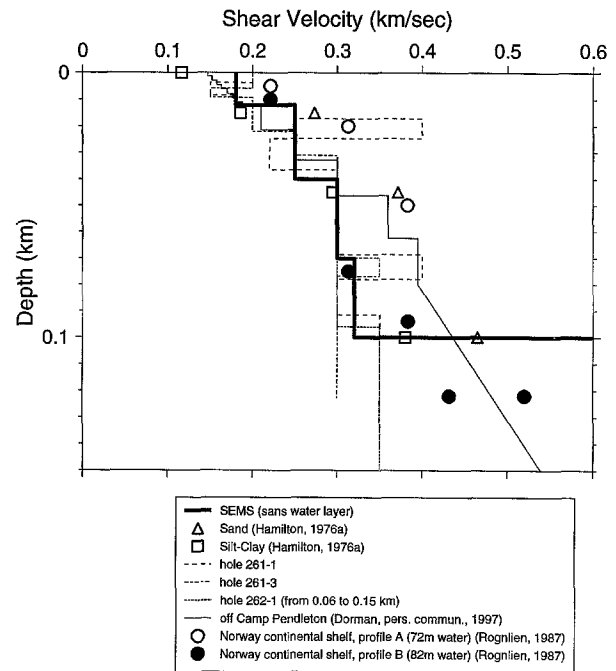


Figure 13. Shear-wave velocity to 0.15 km from offshore sites and adopted SEMS velocity. The velocities for holes 261-1, 261-3, and 262-1 were estimated from standard penetration values near SEMS site S2EE. The velocities for Norwegian sites are point values for a series of representative depths; the actual profiles are characterized by linear velocity gradients with depth.

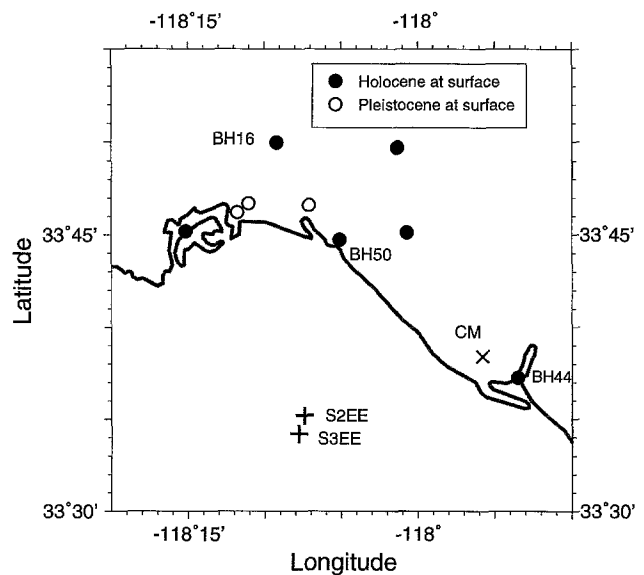


Figure 14. Map of borehole sites (circles) near the SEMS sites offshore of Long Beach (pluses). Boreholes BH16, BH44, and BH50 are discussed in the text; “CM” is the strong-motion station at Costa Mesa (see also Fig. 1).

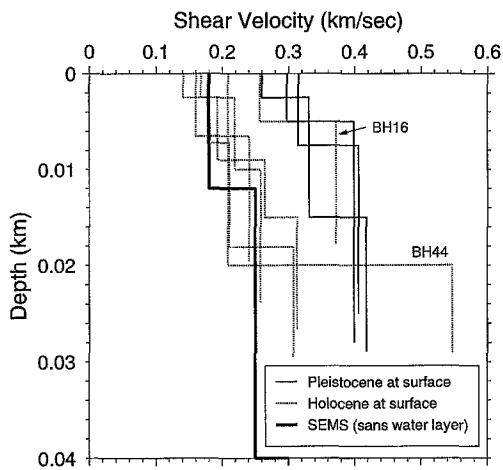


Figure 15. Shear-wave velocity to 0.04 km from borehole sites near Long Beach and for the velocity profile adopted for theoretical calculations at the SEMS sites.

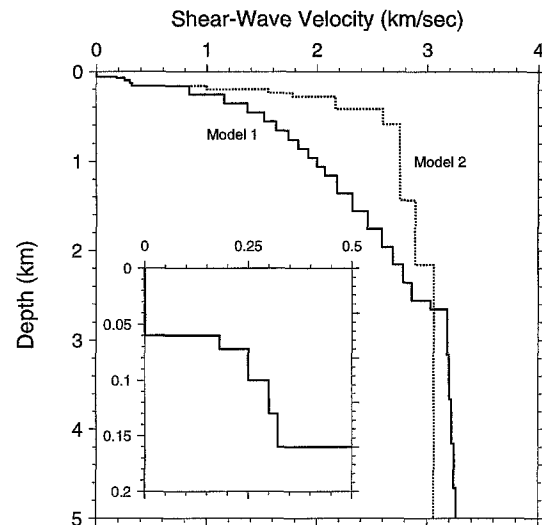


Figure 16. Shear-wave velocity models used in the theoretical calculations.

Another comparison of the SEMS model was previously given in Figure 9, in which the onshore velocities come from farther afield: the Imperial Valley, sites near San Francisco Bay underlain by clay, and Taiwan. The adopted SEMS model has higher velocities near the surface than the clay sites and is in reasonable agreement with the Imperial Valley velocities.

Figures 9 and 15 show that onshore sites exist with velocities similar to those that we have adopted for the offshore sites. It is probably too simplistic to lump sites into simple “offshore” and “onshore” categories. One difference between onshore and offshore sites, however, might be that the subsea depositional environment may lead to less site-to-site variation in the shear-wave velocities near the Earth’s surface.

Crust. The travel time through the upper 100 m of the adopted SEMS model is 0.37 sec. This corresponds to a quarter wavelength period of 1.5 sec. Because we want to do computations out to at least 5.0 sec, it is necessary to specify the velocity structure at deeper depths. We used two models for the material below 100 m: (1) the Magistrale *et al.* (1996) model for the Los Angeles basin, evaluated at the latitude and longitude of station S3EE, and, by way of contrast, (2) the Boore (1986) model for generic California rock (the first author now thinks that the gradient in this model is too steep; he prefers the model of Boore and Joyner, 1997, for generic rock sites). These models were joined to the shallower SEMS model, with the results shown in Figure 16 (showing the shear-wave velocity) and tabulated in Table 5. Model 1 was the primary model used in the calculations.

Results of Theoretical Analysis

We used HSPEC96 (Herrmann, 1996) to do the theoretical modeling. This program uses wavenumber integration

to compute the complete wave field in an earth represented by a stack of laterally uniform, constant-velocity layers. Our procedure was to generate synthetic seismograms for a specified type of faulting for the earth model of interest, and then to treat the synthetic seismogram as we would an observed seismogram. In most cases, we computed the Fourier amplitude spectrum of the *S*-wave portion of the seismogram, although in a few cases, we studied the *P*-wave portion. The focal depth used in the model was 10 km. The surface waves resulting from this depth will not be as energetic as the basin waves, which are probably generated by conversion of body waves at basin edges. For this reason, we do not claim that the theoretical modeling includes basin waves. This is consistent with the possible lack of basin waves in the *V/H* ratios computed from the data (because of the limited duration for some of the SEMS recordings or the presence of noise at long periods).

Comparison of Observed and Theoretical Spectral Ratios. Figure 17 shows the observed and theoretical *V/H* ratios of Fourier amplitude spectra. The observed ratios are for the individual SEMS offshore sites, and the theoretical ratios are geometric averages for a range of focal mechanisms. Although they are somewhat model dependent, the theoretical ratios match the overall trend of *V/H* decreasing with frequency, although they do not predict the precise behavior of the observed ratio at frequencies above about 4 Hz. The ratios at these frequencies are apparently sensitive to details of the site that we are not including in the model. The overall reduction is probably due to refraction of the *S* wave toward the vertical, with a resulting decrease in the *V/H* ratio.

To better understand the influence of different parts of the velocity structure on the observed *V/H* (and in particular, the water layer), we now discuss several calculations com-

Table 5
Velocity Model 1 Used in Theoretical Wave Calculations at Offshore Sites. The First Row is the Water Layer

Thickness	Depth (km)*	VP(km/s)†	VS(km/s)‡	RHO(gm/cc)§	1/QP¶	1/QS
0.060		1.50	0.0	1.0	0.0	0.0
0.012	0.0	1.55	0.18	1.5	0.006	0.063
0.028	0.012	1.65	0.25	2.0	0.006	0.063
0.03	0.04	1.75	0.3	2.0	0.006	0.063
0.03	0.07	1.8	0.32	2.0	0.006	0.063
0.100	0.1	2.02	0.84	2.08	0.0050	0.010
0.100	0.2	2.60	1.16	2.18	0.0040	0.008
0.100	0.3	2.89	1.37	2.22	0.0030	0.006
0.100	0.4	3.09	1.52	2.25	0.0025	0.005
0.100	0.5	3.26	1.63	2.27	0.0020	0.004
0.100	0.6	3.40	1.74	2.30	0.0020	0.003
0.100	0.7	3.53	1.83	2.32	0.0015	0.003
0.100	0.8	3.65	1.92	2.34	0.0015	0.002
0.100	0.9	3.75	2.00	2.36	0.0015	0.002
0.100	1.0	3.85	2.07	2.37	0.0012	0.002
0.200	1.1	3.99	2.18	2.40	0.0010	0.002
0.200	1.3	4.17	2.32	2.44	0.0010	0.002
0.200	1.5	4.36	2.46	2.47	0.0010	0.002
0.200	1.7	4.52	2.59	2.49	0.0010	0.002
0.200	1.9	4.67	2.69	2.52	0.0010	0.002
0.200	2.1	4.82	2.78	2.54	0.0010	0.002
0.200	2.3	4.95	2.86	2.56	0.0010	0.002
0.100	2.5	5.24	3.03	2.65	0.0010	0.002
0.500	2.6	5.50	3.18	2.65	0.0010	0.002
0.500	3.1	5.54	3.20	2.66	0.0010	0.002
0.500	3.6	5.57	3.22	2.67	0.0010	0.002
0.500	4.1	5.61	3.24	2.67	0.0010	0.002
0.500	4.6	5.65	3.26	2.68	0.0010	0.002
0.500	5.1	5.68	3.28	2.68	0.0010	0.002
0.100	5.6	6.00	3.46	2.79	0.0010	0.002
0.400	5.7	6.32	3.65	2.79	0.0010	0.002
0.500	6.1	6.35	3.67	2.80	0.0010	0.001
0.500	6.6	6.38	3.69	2.81	0.0010	0.001
0.500	7.1	6.42	3.71	2.81	0.0004	0.001
0.500	7.6	6.45	3.72	2.82	0.0004	0.001
0.400	8.1	6.48	3.74	2.82	0.0004	0.001
0.100	8.5	6.52	3.77	2.83	0.0004	0.001
1.000	8.6	6.56	3.79	2.84	0.0004	0.001
1.000	9.6	6.58	3.80	2.84	0.0004	0.001
1.500	10.6	6.61	3.81	2.84	0.0004	0.001
1.000	12.1	6.63	3.83	2.85	0.0004	0.001
	13.1	6.65	3.84	2.85	0.0004	0.001

*Depth to the top of the layer; it starts at the seafloor.

†Upper 100 m of sediments: guided by Table A-1b in Hamilton (1976b) for silty clay and clayey silt and by Fumal's (1978) plot of Poisson's ratio vs. shear-wave velocity; below 100 m: from Magistrale et al (1996) model, evaluated at the coordinates of S3EE.

‡Upper 100 m of sediments: guided by the shear-wave velocities determined from standard penetration values at several sites (see text); below 100 m: as in †.

§Upper 100 m: guided by Table A-1b in Hamilton (1976b), Figure 16 in Fumal (1978), and Porcella (1984); below 100 m: as in †.

¶Guided by empirical values and equation (13) in Hamilton (1976c).

||From Liu et al. (1994) for shallow values; deeper values guided by values in Helmberger and McNally (1980) and equation (13) in Hamilton (1976c).

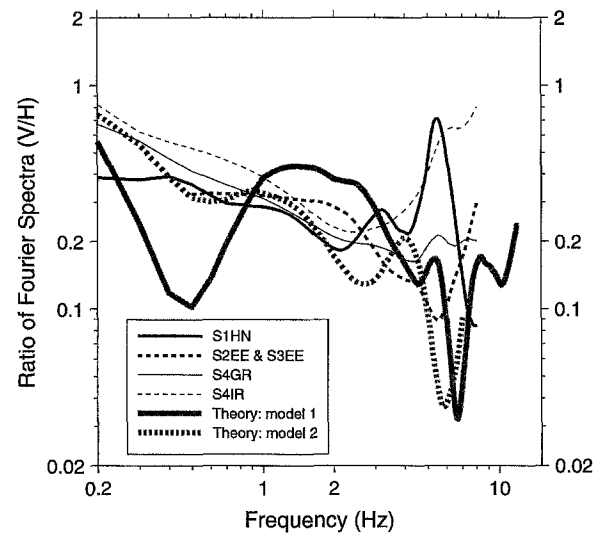


Figure 17. V/H ratios of Fourier amplitude spectra of the S -wave portion of offshore recordings, compared to theoretical predictions.

paring the motions resulting from wave propagation in different permutations of velocity model 1.

Effect of Water Layer. Because shear waves do not propagate through the water layer, the response of vertically incident shear waves should be the same with and without the water layer. For nonvertically incident SV waves, however, conversion of SV to P will occur at the water-soil interface, and the P waves will resonate within the water layer. The converted upgoing P wave will reflect from the ocean surface and travel back down. Some of it will be reflected from the ocean bottom, and some will be converted into downgoing SV waves. A similar process will occur for incident P waves. The wave propagation code HSPEC96 accounts for all of these interactions; it does not assume incidence of a particular type of plane wave; rather, it computes the motion at a given horizontal distance from a point source for a specified type of faulting embedded in the layered structure.

The spectral ratios of motions at the seafloor for model 1 (with a water layer) and at the surface of a model obtained by stripping the water layer off of model 1 are shown in Figure 18. Unlike the previous figure, the ratios in this case are not V/H ; they are ratios of spectra for the same components of motion, with and without the water layer. The spectra were computed for windows that enclosed most of the large-amplitude arrivals. We refer to this as the “ S -wave portion” of the ground motion. As expected, the figure predicts that the water layer exerts almost no influence on the motions in the S -wave portion of the horizontal components. In contrast, the effect of the water layer appears on the S -wave portion of the vertical components for the model with a water layer, as a strong reduction in vertical motion at a particular frequency—an antiresonance. Saying “ S -wave portion” is somewhat misleading, for the wave train starting

around the time of the initial S wave can have P -wave energy, obtained from conversion of S -wave motion to P -wave motion at interfaces (e.g., Takahashi *et al.*, 1992). It is probable that this conversion of S -wave motion into P -wave motion at the seafloor is leading to the reduction in vertical motions compared to the case with no water layer (Bureau, 1986, also did calculations that yielded a reduction in vertical motion for an ocean-bottom site). The frequency at which the reduction in S energy is greatest is the fundamental resonance mode for P waves trapped in the water layer. At offshore sites, this water-layer effect on the vertical component of the S wave will lead to different theoretical V/H ratios for onshore and offshore sites underlain by the same materials, but the difference will only be pronounced for frequencies greater than about one-half the water-layer resonance frequency. At onshore sites, the P waves converted from S waves might resonate between the surface and the interface formed by the large contrast in P velocity across the water table (e.g., Mueller *et al.*, 1982), increasing the V/H ratio for onshore sites.

As mentioned earlier, the water layer will have its most pronounced effect on motions dominated by P waves. Crouse and Quilter (1991) give a simple theory that predicts the ratio of P -wave motion at the seafloor relative to motion without the overlaying water layer. The largest effect should be at frequencies corresponding to resonance in the water layer. At resonance, a phase change at the water–seafloor interface leads to destructive interference and a relative node in the P -wave motion. Only the fundamental mode is in the frequency range of our data. The resonant frequency is given by $f_p = C/(4H)$, where C is the velocity of P waves in water (1500 m/sec) and H is the water thickness. For a depth of 60 m (200 ft), this gives $f_p = 6.25$ Hz. For nonvertical wave propagation, the P -wave velocity should be replaced by the apparent vertical velocity; this will be somewhat larger than the velocity used in our calculation, leading to a higher resonant frequency. We used HSPEC96 to check the model of Crouse and Quilter. The results are shown in Figure 19, from which it can be seen that their simple theory is in good agreement with the calculations. Based on these results, we can conclude that the water layer itself will not affect seafloor motions for frequencies lower than about $f_p/2$. For platforms near the SEMS stations providing the data analyzed in this article, we do not expect the water layer itself to influence directly waves with frequencies less than about 3 Hz. Of course, as the water depth increases, the resonant frequency moves to smaller values (but so does the resonant frequency of a platform), so that for the deepest SEMS site (S4EU), we expect frequencies of 1.7 Hz and higher to be affected by resonance in the water layer. No data are available for S4EU.

Effect of Soil Layer. Figure 20 shows the ratio of Fourier amplitude spectra of S -wave motions for the model with and without the first 100 m of low-velocity sediments (in both cases, the water layer has been removed). Ratios are shown for horizontal and for vertical components. Clearly, the soft

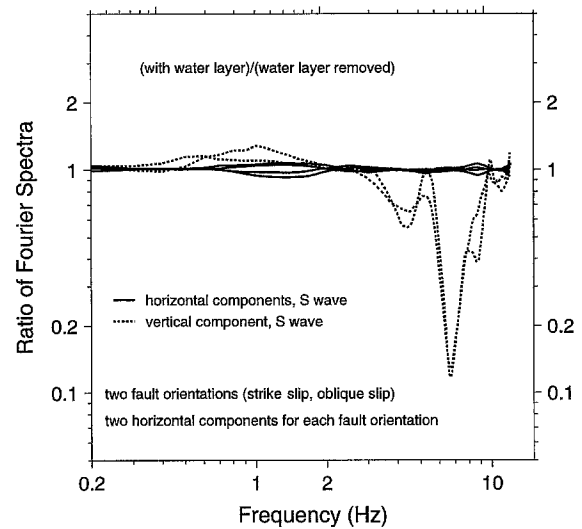


Figure 18. Ratios of Fourier spectra for a window including the S -wave portion of horizontal-component (solid lines) and vertical-component (dashed lines) synthetic seismograms computed for various velocity models and fault orientations (because the results are so similar, the different orientations are not specifically identified). Shown are the ratio of spectra for models with and without the water layer.

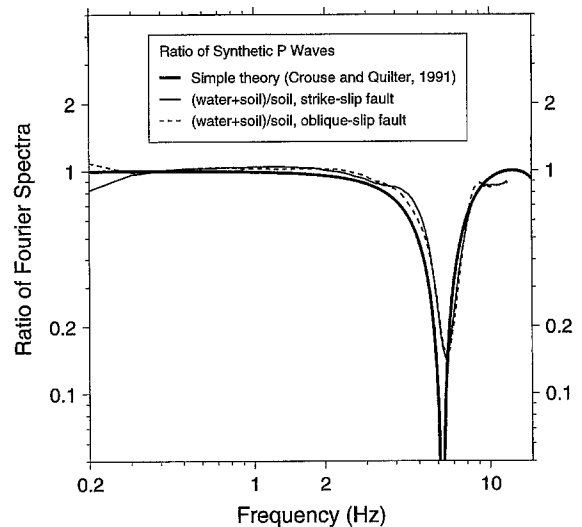


Figure 19. Ratios of Fourier spectra for the P -wave portion of vertical-component synthetic seismograms computed for various velocity models and fault orientations. Spectral ratios were computed after smoothing each component with a triangular operator spanning 2 Hz. Also shown is the prediction from a simple model of a P -wave vertically incident on a water layer overlying an elastic half-space (Crouse and Quilter, 1991).

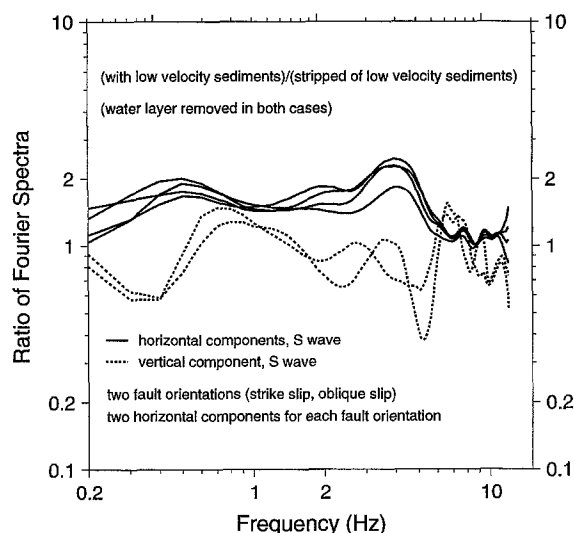


Figure 20. Ratios of Fourier spectra for the S -wave portion of horizontal-component (solid lines) and vertical-component (dashed lines) synthetic seismograms computed for various velocity models and fault orientations (because the results are so similar, the different orientations are not specifically identified). Shown are the ratio of spectra for models with and without the upper 0.1 km of sediments, with the water layer removed in both cases.

sediments have a pronounced affect on the motions for the horizontal component, even for frequencies as low as 0.4 Hz, where the amplifications approach a factor of 2. The high-frequency behavior of the horizontal-component ratios reflects a trade-off between increased attenuation and amplification in the low-velocity sediments, relative to the model with no soft sediments.

Conclusions and Discussion

The Seafloor Earthquake Measuring System (SEMS) is an instrumentation effort that has been in existence for almost two decades. The SEMS stations are excellent instruments and have produced high-quality data for a number of events. Unfortunately, until recently, onshore strong-motion instruments have not generally been of the same high caliber as the SEMS units, and therefore, few data are available from which direct comparisons can be made of onshore and offshore motions from the same earthquake recorded at similar distances and for similar site conditions. For this reason, the analysis of the SEMS data has had to use a combination of somewhat indirect observational studies and theoretical calculations to answer the fundamental question: Are the earthquake ground motions at the seafloor so different from onshore motions that the more numerous onshore recordings cannot be used for platform design?

The answer to the fundamental question is "It depends." It depends on the component of motion and the frequency of ground shaking. The ratio of vertical-to-horizontal mo-

tions (V/H) is clearly much smaller than for onshore recordings at relatively high frequencies (above about 3 Hz). Studies of the vertical and horizontal motions separately show that the anomaly lies with the vertical motions. For lower frequencies, the results of this study suggest that both components of the seafloor motions are similar to those from onshore recordings at sites underlain by geologic materials similar to those beneath the seafloor sites.

Theoretical studies show that the reduction of vertical motions can be produced by interactions of S waves in the solid materials below the seafloor and P waves in the water layer. This interaction is most important at the resonant frequencies of vertically propagating acoustic waves in the water layer. A reduced vertical component can also be produced by refraction of an incoming wave toward the vertical, such as will occur for shear-wave velocities that decrease toward the Earth's surface.

The water layer indirectly influences motions by allowing low-velocity sediments to exist over a widespread area and by increasing the pore pressure in the sediments, which will reduce the velocity in sands and silts.

The water layer and the near-surface shear-wave velocities lead to complexities in the high-frequency motions. Although some parts of the platform system are sensitive to these high-frequency motions (e.g., Smith, 1994; Brady, 1993), the frequencies are generally much higher than the horizontal resonance frequencies of the platform. More important for design and analysis of platforms are periods of motion longer than 1 sec.

Particularly useful recordings for the study of long-period motions were made at a SEMS site offshore of Long Beach. Time-domain comparisons with onshore waves that have traveled through the Los Angeles basin suggest that the seafloor motions at the SEMS site are significantly influenced by late-arriving, large-amplitude surface waves (basin waves) at long periods. These waves may be more important for platform analysis and design than the higher frequency waves that are influenced by the water layer. In this sense, the travel path may be more important than the local site conditions.

Acknowledgments

We wish to thank the many people who contributed data, information, or criticisms. These include Norm Abrahamson, Gail Atkinson, Yousef Bozorgnia, Hilmar Bungum, C. B. Crouse, Leroy Dorman, Joe Ehasz, Tom Fumal, Jim Gibbs, Jens Havskov, Bob Herrmann, Francois Heuze, Bill Joyner, Hiroshi Kawase, Harold Magistrale, Farrokh Nadim, Dan O'Connell, Linda Seekins, Gerry Sleaf, Kuo-Liang Wen, and Bob Yerkes. The strong-motion programs of the California Division of Mines and Geology and the U.S. Geological Survey provided accelerograms and borehole velocities. Raul Castro and an anonymous reviewer provided useful comments. This work was partially funded by the Minerals Management Service.

References

- Abrahamson, N. A. and W. J. Silva (1997). Empirical response spectral attenuation relations for shallow crustal earthquakes, *Seism. Res. Lett.* **68**, 94–127.

- Anderson, J. G., M. D. Trifunac, T.-L. Teng, A. Amini, and K. Moslem (1981). Los Angeles vicinity strong motion accelerograph network, Civil Engineering Report CE 81-04, Univ. of Southern California, 79 pp.
- Atakan, K. and J. Havskov (1996). Local site effects in northern North Sea based on single-station spectral ratios of OBS recordings, *Terra Nova* **8**, 22–33.
- Boore, D. M. (1986). Short-period *P*- and *S*-wave radiation from large earthquakes: implications for spectral scaling relations, *Bull. Seism. Soc. Am.* **76**, 43–64.
- Boore, D. M. (1997). Analysis of earthquake recordings obtained from the Seafloor Earthquake Measurement System (SEMS) instruments deployed off the coast of southern California, *U.S. Geol. Surv. Open-File Rept. 97-733*, 242 pp.
- Boore, D. M. and W. B. Joyner (1997). Site-amplifications for generic rock sites, *Bull. Seism. Soc. Am.* **87**, 327–341.
- Bozorgnia, Y. and M. Niazi (1993). Distance scaling of vertical and horizontal response spectra of the Loma Prieta earthquake, *J. Earthquake Eng. Structural Dyn.* **22**, 695–707.
- Bozorgnia, Y., M. Niazi, and K. W. Campbell (1994). Vertical ground motion during the 1994 Northridge earthquake, *Proc. of 6th U.S.–Japan Workshop on the Improvement of Building Structural Design and Practices*, ATC-15-5, Applied Technology Council, Redwood City, California.
- Bozorgnia, Y., M. Niazi, and K. W. Campbell (1995). Characteristics of free-field vertical ground motion during the Northridge earthquake, *Earthquake Spectra* **11**, 515–525.
- Brady, A. G. (1993). Offshore strong ground motion and onshore surrogates, *Proc. International Workshop on Wind and Earthquake Engineering for Offshore and Coastal Facilities*, Yokosuka, Japan, May 12–14.
- Bureau, G. (1986). New considerations for offshore seismic response studies, *Proc. of the Third U.S. National Conf. on Earthquake Engineering*, Charleston, South Carolina, Vol. 1, 789–795.
- Campbell, K. W. (1997). Empirical near-source attenuation relationships for horizontal and vertical components of peak ground acceleration, peak ground velocity, and pseudo-absolute acceleration response spectra, *Seism. Res. Lett.* **68**, 154–179.
- Chen, J., R. R. Ullmann, and A. B. Mason (1989). Measurement of earthquake ground acceleration and structural response of a fixed offshore platform, *Proc. Offshore Technology Conference*, OTC 6172, 561–568.
- Crouse, C. B. and J. Quilter (1991). Seismic hazard analysis and development of design spectra for Maui A platform, *Proc. Pacific Conf. on Earthquake Engineering*, New Zealand, Vol. 3, 137–148.
- Fumal, T. E. (1978). Correlations between seismic wave velocities and physical properties of near-surface geologic materials in the southern San Francisco Bay region, California, *U.S. Geol. Surv. Open-File Rept. 78-1067*, 114 pp.
- Hamilton, E. L. (1976a). Shear-wave velocity versus depth in marine sediments: a review, *Geophysics* **41**, 985–996.
- Hamilton, E. L. (1976b). Variations of density and porosity with depth in deep-sea sediments, *J. Sedimentary Petrol.* **46**, 280–300.
- Hamilton, E. L. (1976c). Attenuation of shear waves in marine sediments, *J. Acoust. Soc. Am.* **60**, 334–338.
- Helmberger, D. and K. McNally (1980). Attenuation of shear waves in marine sediments: Santa Barbara Channel, Woodward Clyde & Assoc. Report to Sandia Laboratories.
- Herrmann, R. B. (1996). *Computer Programs in Seismology: An Overview of Synthetic Seismogram Computation (Version 3)*, Dept. of Earth and Atmospheric Sciences, St. Louis University, St. Louis, Missouri.
- Hudson, D. E. (1979). *Reading and Interpreting Strong Motion Accelerograms*, Earthquake Engineering Research Institute, Berkeley, California, 112 pp.
- Liu, H.-P., R. E. Warrick, R. E. Westerlund, and R. E. Kayen (1994). *In situ* measurement of seismic shear-wave absorption in the San Francisco Holocene Bay Mud by the pulse broadening method, *Bull. Seism. Soc. Am.* **84**, 62–75.
- Magistrale, H., K. McLaughlin, and S. Day (1996). A geology based 3D velocity model of the Los Angeles basin sediments, *Bull. Seism. Soc. Am.* **86**, 1161–1166.
- Mason, A. B., J. L. Beck, J. Chen, and R. R. Ullmann (1989). Modal parameter identification of an offshore platform from earthquake response records, *Seismic Engineering: Research and Practice, Proceedings of Structures Congress '89*, American Society of Civil Engineers, 217–226.
- Mueller, C. S., D. M. Boore, and R. L. Porcella (1982). Detailed study of site amplification at El Centro strong-motion array station #6, *Proc. of the Third Int. Conf. on Earthquake Microzonation*, 1, Seattle, Washington, June 28–July 1, 1982, 413–424.
- Niazi, M. and Y. Bozorgnia (1992). Behavior of near-source vertical and horizontal response spectra at SMART-1 array, Taiwan, *J. Earthquake Eng. Structural Dyn.* **21**, 37–50.
- Porcella, R. L. (1984). Geotechnical investigations at strong-motion stations in the Imperial Valley, California, *U.S. Geol. Surv. Open-File Rept. 84-562*, 174 pp.
- Reece, E. W., D. E. Ryerson, and R. L. McNeill (1981). Long-term measurements of ground motions offshore, *International Conf. on Recent Advances in Geotechnical Earthquake Engineering and Soil Dynamics*, St. Louis, Missouri, April 26–May 3, 1981, Vol. I, 377–380.
- Rognlien, B. (1987). Soil response on selected sites on the Norwegian continental shelf, ELOCS Report 4-1.
- Ryerson, D. E. (1981). Seafloor earthquake measurement system, Vol. 1, Overview and physical description, Sandia Report SAND81-1810/1, 66 pp.
- Sleefe, G. E. (1990). The long-term measurement of strong-motion earthquakes offshore southern California, *Proc. Offshore Technology Conference*, OTC 6336, 561–568.
- Sleefe, G. E. and D. Engi (1987). Seafloor response for two southern California earthquakes, *Proc. 1987 Spring Conf. on Exper. Mech.*, Houston, Texas, June 14–19, 1987, and Sandia report SAND86-2441C.
- Smith, C. E. (1990). Seismic design considerations for offshore oil and gas structures, *Proc. 21st Joint Meeting of the U.S.–Japan Cooperative Program in Natural Resources: Panel on Wind and Seismic Effects*, NIST SP 776.
- Smith, C. E. (1991). Seafloor seismic network offshore southern California, *Proc. 23rd Joint Meeting of the U.S.–Japan Cooperative Program in Natural Resources: Panel on Wind and Seismic Effects*.
- Smith, C. E. (1994). Dynamic response of offshore steel-jacket platforms subject to measured seafloor seismic ground motions, *Ph.D. Thesis*, Graduate School of Engineering and Applied Science, George Washington University, 323 pp.
- Takahashi, K., S. Ohno, M. Takemura, T. Ohta, Y. Sugawara, T. Hatori, and S. Omote (1992). Observation of earthquake strong-motion with deep borehole: generation of vertical motion propagating in surface layers after *S* arrival, *Proc. Tenth World Conf. on Earthquake Engineering*, Balkema, Rotterdam, 1245–1250.

U.S. Geological Survey
345 Middlefield Road
Menlo Park, California 94025
dboore@isdmnl.wr.usgs.gov
(D.M.B.)

Minerals Management Service
Herndon, Virginia 20170
csmith@mms.gov
(C.E.S.)